Electrochemistry Communications 77 (2017) 28–31

Contents lists available at ScienceDirect

Electrochemistry Communications

journal homepage: www.elsevier.com/locate/elecom

Roles of positive or negative electrodes in the thermal runaway of lithium-ion batteries: Accelerating rate calorimetry analyses with an all-inclusive microcell

Takao Inoue, Kazuhiko Mukai *

Toyota Central Research & Development Laboratories, Inc., 41-1 Yokomichi, Nagakute, Aichi 480-1192, Japan

ARTICLE INFO

Article history:
Received 18 January 2017
Received in revised form 6 February 2017
Accepted 7 February 2017
Available online 11 February 2017

Keywords:
Lithium-ion battery
Thermal runaway
Accelerating rate calorimetry
Differential scanning calorimetry
Exothermic reaction

ABSTRACT

To improve the thermal stability of lithium-ion batteries (LIBs) at elevated temperatures, the roles of positive or negative electrode materials in thermal runaway should be clarified. In this paper, we performed accelerating rare calorimetry analyses on two types of LIBs by using an all-inclusive microcell (AIM) method, where the AIM consists of all LIB components. We found that the thermal runaway in $LiNi_{0.8}Co_{0.15}Al_{0.05}O_2$ (NCA)|$LiPF_6$ dissolved in ethylene carbonate (EC)/diethyl carbonate solution (DEC) (EC/DEC = 1/1 by volume); $LiPF_6$(EC/DEC)|artificial graphite (AG) and $LiNi_{1/3}Co_{1/3}Mn_{1/3}O_2$ (NCM)|$LiPF_6$(EC/DEC)|AG cells is brought about by different electrodes, i.e., NCA for the former, and AG for the latter. The above difference is attributed to the different oxidation temperature of the EC/DEC solvents, indicating that we first pay attention which electrodes govern the thermal runaway. Trials for improving the thermal stability of NCA are also reported.

© 2017 Elsevier B.V. All rights reserved.

1. Introduction

Thermal runaway at elevated temperatures (T) in lithium-ion batteries (LIBs) is one of the biggest issues for their applications to electric vehicles and stationary energy storage systems [1–6]. To elucidate the mechanism of thermal runaway, accelerating rate calorimetry (ARC) analyses have been employed because they provide an adiabatic self-heating rate as a function of time (t), i.e., $\Delta T/\Delta t$ [7]. Among the numerous ARC studies on LIBs, research efforts have been focused on exothermic reactions between positive electrode materials and electrolytes, for instance, on the x dependence of $\Delta T/\Delta t$ for Li_xCoO_2 (LCO) and $Li_xNi_pMn_qCo_rO_2$ [8–10], the effects of electrolyte quantities on LCO and $Li_xMn_2O_4$ [11], the effects of electrolyte additives for $Li_xNi_{0.8}Co_{0.15}Al_{0.05}O_2$ (NCA) and $Li_xNi_{1/3}Co_{1/3}Mn_{1/3}O_2$ (NCM) [12,13], and the effects of different particle morphologies or electrode densities for NCA and Li_xFePO_4 [14–16]. This is probably because thermal runaway in LIBs is considered to be mainly caused by exothermic reactions between positive electrodes and electrolytes based on ARC studies of laboratory-made full-cells [17,18]. However, the temperature dependence of $\Delta T/\Delta t$ for a negative electrode material, Li_xC_6 [19–21] is similar with those for LCO [8,9,11] and NCA [12,13]. Hence, the roles of positive or negative electrode materials in thermal runaway are still not fully understood, particularly for LIBs consisting of LCO (NCA) and graphite.

Recently, we developed an all-inclusive microcell (AIM) for differential scanning calorimetry (DSC) analyses for two types of LIBs. That is, NCA|1 M $LiPF_6$ dissolved in ethylene carbonate (EC)/diethyl carbonate (DEC) (1/1 by volume) solution, hereafter denoted as $LiPF_6$(EC/DEC)|artificial graphite (AG) and NCM|$LiPF_6$(EC/DEC)|AG [22]. Here the AIM consists of all LIB components so it works as a battery itself, and it reveals contributions from each exothermic reaction to the total heat generation (ΔH). Consequently, we found that the exothermic reaction between Li_xC_6 and $LiPF_6$ at around 260 °C significantly influences subsequent exothermic reactions and ΔH in NCA|$LiPF_6$(EC/DEC)|AG and NCM|$LiPF_6$(EC/DEC)|AG [22]. By applying the AIM method to ARC analyses, we expect to obtain crucial information about the roles of positive or negative electrode materials in thermal runaway.

In this paper, we performed ARC studies on NCA|$LiPF_6$(EC/DEC)|AG and NCM|$LiPF_6$(EC/DEC)|AG cells using the AIM method to clarify whether NCA (NCM) or AG governs the thermal runaway in these cells. Accordingly, NCA is found to govern the thermal runaway for the former cell, whereas AG for the latter cell, due to the difference in the oxidation T of the EC/DEC solvents. We also conducted a trial for improving the thermal stability of NCA by using electrode additives.

* Corresponding author.
E-mail address: e1089@mosk.tytlabs.co.jp (K. Mukai).

http://dx.doi.org/10.1016/j.elecom.2017.02.008
1388-2481/© 2017 Elsevier B.V. All rights reserved.

2. Experimental

NCA, NCM, and AG samples were provided by Sakai Chemical Industry Co., Ltd., Toda Kogyo Corp., and Osaka Gas Chemicals Co., Ltd., respectively. The $LiPF_6$(EC/DEC) electrolyte and the polyethylene (PE) separator were obtained from Kishida Chemical Co., Ltd. and Toray Battery Separator Film Co., Ltd., respectively. Two types of LIBs with ~750 mAh were constructed: NCA|$LiPF_6$(EC/DEC)|AG and NCM|$LiPF_6$(EC/DEC)|AG. The positive electrode consisted of 85 wt% NCA (NCM), 10 wt% acetylene black (AB, Denka Company Ltd.), and 5 wt% polyvinylidene fluoride (PVdF, Kureha Corp.). The negative electrode consisted of 95 wt% AG and 5 wt% PVdF. Further information about the fabrication of the LIBs is given elsewhere [22]. To improve the thermal stability of delithiated NCA, MgB_2 or AlB_2 powder (Koujyundo Chemical Laboratory, Co., Ltd.) was mixed with the NCA electrode. The electrode consisted of 85 wt% NCA, 5 wt% AB, 5 wt% MgB_2 (AlB_2), and 5 wt% PVdF. For this purpose, we used 1 M $LiPF_6$ dissolved in EC/DEC/ethylmethyl carbonate (EMC) (3/3/4 by volume) [$LiPF_6$(EC/DEC/EMC)] solution, as an electrolyte.

The delithiated NCA (or NCM) and lithiated AG samples for the ARC measurements were prepared by charging each LIB up to 4.1 V (SOC = 100%), using a constant-current (CC) and constant-voltage (CV) mode. The duration of the CC-CV mode was 7 h. The applied current was 100 mA (0.13 °C), which corresponds to a current density of ~0.21 $mA \cdot cm^{-2}$, based on the surface area of the positive electrode. After disassembling each LIB, 200 (150) mg of the positive (negative) electrode was removed for the ARC measurements. The ARC measurements were conducted with a heating step of 5 °C starting from 50 °C (esARC, Thermal Hazard Technology Co.). Before starting the measurements, we calibrated four thermocouples of the ARC apparatus and confirmed that the onset T of self-heating for di-tert-butyl peroxide was between 120 and 140 °C. The NCA (NCM) electrode together with 94 μL of $LiPF_6$(EC/DEC) was installed in a stainless steel pipe (SUS304), which was 10 mm in diameter and 70 mm in height, and weighed 1.5 g (= 0.885 $J \cdot K^{-1}$). For the AG electrode, 86 μL of $LiPF_6$(EC/DEC) was installed in the SUS pipe. Furthermore, for the AIM analyses, the NCA (NCM) electrode, the AG electrode, and 182 μL of $LiPF_6$(EC/DEC) were installed in the SUS pipe. The amounts of the electrolyte were determined by those of commercial LIBs. The T rate sensitivity was 0.02 °C·min^{-1} and the holding time was 6 min. This means that when $\Delta T/\Delta t$ is <0.02 °C·min^{-1} within 6 min of holding time, the next heating step (= 5 °C) proceeds. Otherwise, the T of the ARC circumstance is increased corresponding to that of the SUS pipe to maintain adiabatic conditions.

The thermal stability of NCA containing MgB_2 (AlB_2) was examined by DSC (Thermo plus EVO2, DSC8230L, Rigaku Co. Ltd.) analyses with a heating rate of 5 °C·min^{-1}.

3. Results and discussion

Fig. 1 shows the initial charge and discharge (C/D) curves of the NCA|$LiPF_6$(EC/DEC)|AG and NCM|$LiPF_6$(EC/DEC)|AG cells. The voltage for NCA rapidly increases from ~2 V at the beginning of the charge reaction, and then gradually increases to 4.1 V with several plateaus appearing around 3.5 and 3.6 V. The charge capacity (Q_{cha}) is 181.7 mAh·g^{-1}, and the discharge capacity (Q_{dis}) is 140.0 mAh·g^{-1}. The Li compositions (x) for the ARC analyses were 0.34(1) in $Li_xNi_{0.8}Co_{0.15}Al_{0.05}O_2$ and 0.60(1) in Li_xC_6. The C/D curves for NCM shift to a slightly higher voltage region than for NCA. This is due to the difference in redox species between NCA and NCM; i.e., mainly $Ni^{3+} \leftrightarrow Ni^{4+}$ ions for NCA [23], but mainly $Ni^{2+} \leftrightarrow Ni^{3+} \leftrightarrow Ni^{4+}$ and $Co^{3+} \leftrightarrow Co^{4+}$ for NCM [24]. The initial Q_{cha} and Q_{dis} for NCM are 166 and 139 mAh·g^{-1}, respectively. The x values for the ARC analyses were 0.39(1) in $Li_xNi_{1/3}Co_{1/3}Mn_{1/3}O_2$ and 0.57(1) in Li_xC_6.

Fig. 2(a) shows the T dependence of $\Delta T/\Delta t$ for NCA, AG, and NCA|$LiPF_6$(EC/DEC)|AG (= AIM). Each corresponding DSC curve, taken from Ref. [22], is also shown in Fig. 2(b) for comparison. The $\Delta T/\Delta t$ for NCA starts to rapidly increase at ~120 °C, then exhibits a maximum at around 160 °C, and finally increases again above 200 °C. The maximum around 160 °C and the increase in $\Delta T/\Delta t$ above 200 °C correspond to the exothermic reactions in the DSC curve at around 200 and 240 °C, respectively, where both exothermic reactions are attributed to the reactions between the released oxygen (δO_2) from the NCA lattice and the EC/DEC solvent [14,22,25]:

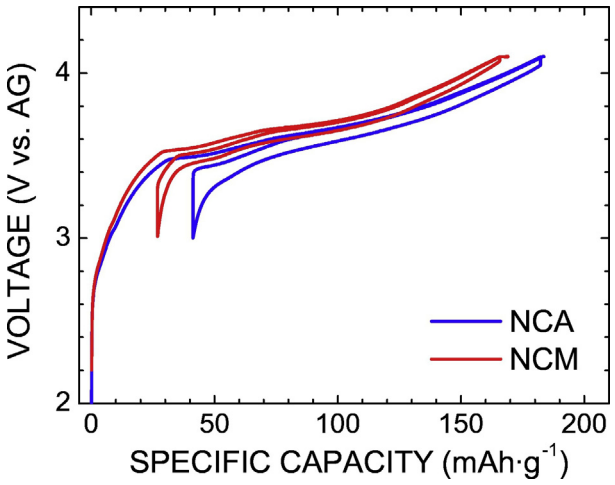

Fig. 1. Charge and discharges curves of $LiNi_{0.8}Co_{0.15}Al_{0.05}O_2$ (NCA)|$LiPF_6$(EC/DEC)|AG and $LiNi_{1/3}Co_{1/3}Mn_{1/3}O_2$ (NCM)|$LiPF_6$(EC/DEC)|AG cells, which were operated at a current of 100 mA (≈0.21 mA·cm^{-2}).

$$\delta/5C_3H_4O_3 + \delta/2O_2 \rightarrow 3\delta/5CO_2 + 2\delta/5H_2O \quad (1)$$

and

$$\delta/12C_5H_{10}O_3 + \delta/2O_2 \rightarrow 5\delta/12CO_2 + 5\delta/12H_2O. \quad (2)$$

Meanwhile, the $\Delta T/\Delta t$ curve for AG does not show any significant increase below 200 °C, but shows two distinct increases at 200 °C ≤ T ≤ 260 °C and T > 260 °C. Based on the exothermic reactions in the DSC curve for AG, the increase in $\Delta T/\Delta t$ at 200 °C ≤ T ≤ 260 °C is attributable to the reaction between Li_xC_6 and the $LiPF_6$ salt [22,26]:

$$5Li_xC_6 + xPF_5 \rightarrow 5xLiF + xP + 5C_6, \quad (3)$$

and the increase in $\Delta T/\Delta t$ at T > 260 °C is attributable to the reaction between Li_xC_6 and the EC/DEC solvent [22,26]:

$$4Li_xC_6 + xC_3H_4O_3 + xC_5H_{10}O_3 \rightarrow 2xLi_2CO_3 + 2xC_2H_4 + xC_2H_6 + 4C_6. \quad (4)$$

The $\Delta T/\Delta t$ curve for the AIM is similar to that for NCA except for the maximum at around 160 °C. The difference is probably due to an endothermic melting reaction of the PE separator at around 135 °C [see Fig. 2(b)]. The similarity in the $\Delta T/\Delta t$ curve between the AIM and NCA with the electrolyte indicates that the thermal runaway in NCA|$LiPF_6$(EC/DEC)|AG is mainly triggered by the exothermic reactions at around 200 °C described in Eqs. (1) and (2). In other words, the NCA electrode governs the thermal runaway in NCA|$LiPF_6$(EC/DEC)|AG.

Fig. 3(a) shows the T dependence of $\Delta T/\Delta t$ for NCM, AG, and NCM|$LiPF_6$(EC/DEC)|AG (= AIM). Each corresponding DSC curve, taken from Ref. [22], is also shown in Fig. 3(b) for comparison. The $\Delta T/\Delta t$ for NCM increases rapidly above ~300 °C, although several spikes below 1 °C·min^{-1} are seen at T ≤ ~300 °C. The rapid increase in $\Delta T/\Delta t$ above 300 °C corresponds to an exothermic peak at ~315 °C in the DSC curve, as shown in Fig. 3(b). This exothermic reaction is attributed to reactions between the released oxygen (δO_2) from the NCM lattice and the EC/DEC solvent, as described in Eqs. (3) and (4). Note that

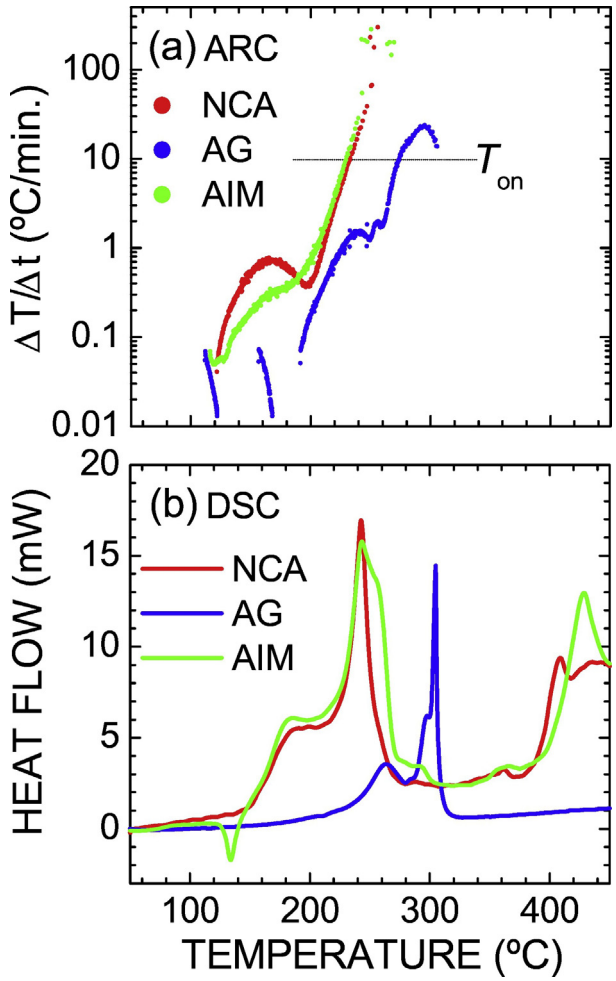

Fig. 2. (a) Temperature dependence of $\Delta T/\Delta t$ for NCA, AG, and NCA|LiPF$_6$(EC/DEC)|AG (=AIM). The NCA and AG samples contain the LiPF$_6$(EC/DEC) electrolyte. Each corresponding DSC profile, taken from Ref. [22], is shown in (b) for comparison. The onset temperature (T_{on}) for the thermal runaway is defined as the temperature at which $\Delta T/\Delta t \geq 10\ °C \cdot min^{-1}$.

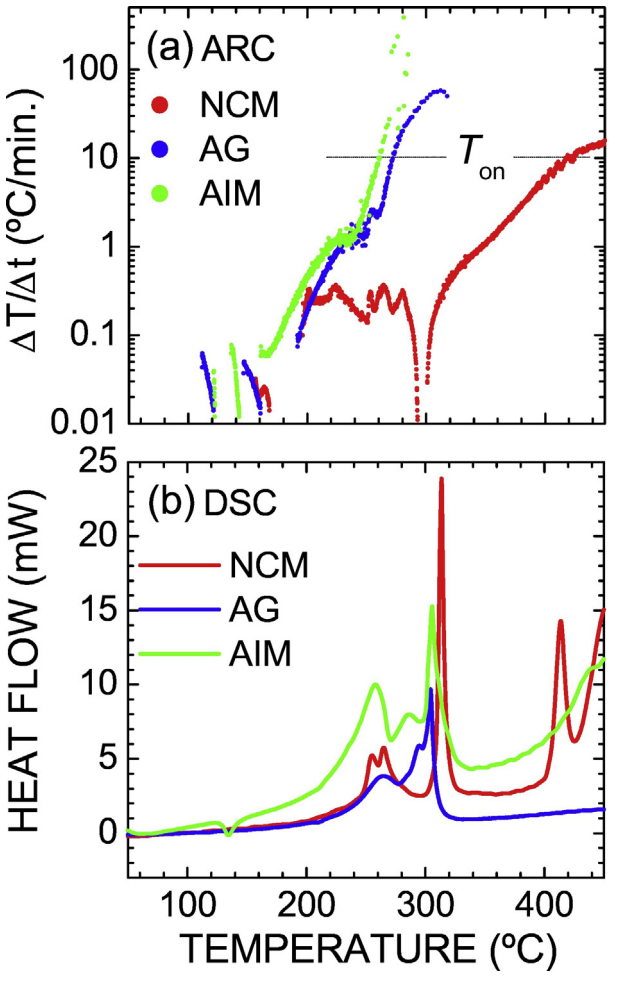

Fig. 3. (a) Temperature dependence of $\Delta T/\Delta t$ for NCM, AG, and NCM|LiPF$_6$(EC/DEC)|AG (=AIM). NCM and AG samples contain the LiPF$_6$(EC/DEC) electrolyte. Each corresponding DSC profile, taken from Ref. [22], is shown in (b) for comparison. The onset temperature (T_{on}) for the thermal runaway is defined as the temperature at which $\Delta T/\Delta t \geq 10\ °C \cdot min^{-1}$.

the exothermic reaction between the released oxygen and EC/DEC occurs at ~240 °C for NCA [see Fig. 2(b)], which is ~60 °C lower than that for NCM. The difference between NCA and NCM is caused by the difference in the T of a phase transition into a rock-salt structure, as reported previously [22,24,27]. Consequently, the $\Delta T/\Delta t$ curve for the AIM resembles that for AG, indicating that the thermal runaway in NCM|LiPF$_6$(EC/DEC)|AG is mainly triggered by the exothermic reaction at around 260 °C described in Eq. (3). Hence, the AG (negative) electrode governs the thermal runaway in NCM|LiPF$_6$(EC/DEC)|AG.

Based on the ARC and DSC results, the reaction scheme of the thermal runaway in NCA|LiPF$_6$(EC/DEC)|AG and NCM|LiPF$_6$(EC/DEC)|AG is summarized in Fig. 4. For NCA|LiPF$_6$(EC/DEC)|AG, the self-heating rate increases from ~115 °C, and the thermal runaway occurs above ~230 °C (= T_{on}) due to oxidation of the EC/DEC solvent. Here T_{on} is defined as T at which $\Delta T/\Delta t \geq 10\ °C \cdot min^{-1}$ [see Figs. 2(a) and 3(a)] according to the limitation of accuracy of the present ARC system. In contrast, the thermal runaway in NCM|LiPF$_6$(EC/DEC)|AG occurs above ~260 °C (= T_{on}), which is caused by the formation of LiF. The difference between NCA and NCM is whether the oxidation T of the solvents is higher or lower than the T for the formation of LiF. Thus, to suppress the thermal runaway in NCA|LiPF$_6$(EC/DEC)|AG (or NCM|LiPF$_6$(EC/DEC)|AG), the thermal stability of the NCA (or AG) electrode should be improved. Other than the above-mentioned LIBs, ARC analyses with the AIM method would also be applicable for various LIBs, such as LMO + AG and LCO + Li[Li$_{1/3}$Ti$_{5/3}$]O$_4$ combinations. However, the information about whether the positive or the negative electrode material governs the thermal runaway is obtained only by examining three sets of ARC data, i.e., data for a positive electrode, data for a negative electrode, and data for an AIM. Combined with the DSC data for each component, the exothermic reaction leading to the thermal runaway can be revealed.

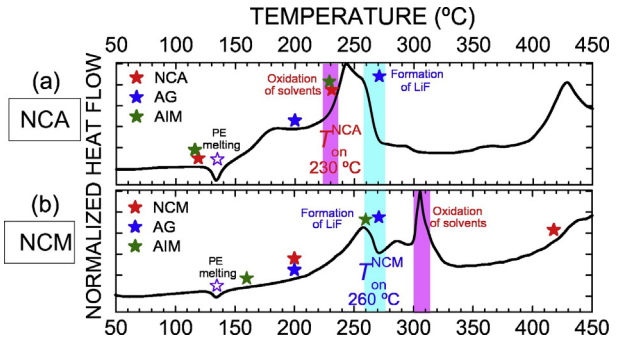

Fig. 4. The reaction mechanism of thermal runaway for the (a) NCA|LiPF$_6$(EC/DEC)|AG and (b) NCM|LiPF$_6$(EC/DEC)|AG cells. Closed stars indicate the onset temperatures for various exothermic reactions, while the open star at ~130 °C indicates the temperature of the endothermic reaction on the PE separator. The normalized DSC curves of AIM are shown to clarify the thermal stability of both cells.

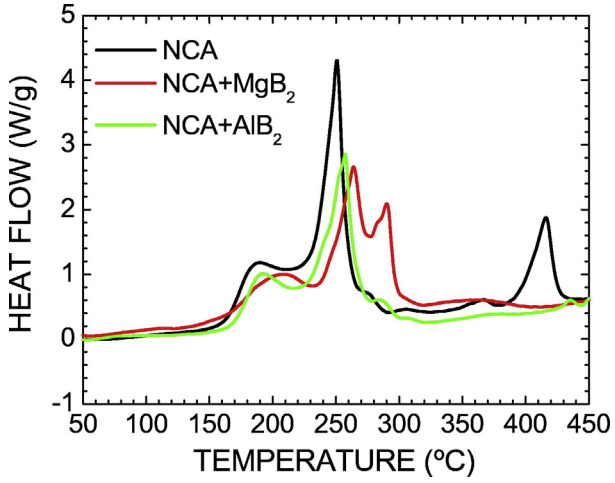

Fig. 5. Trial for improving the thermal stability of NCA: DSC curves for NCA, NCA + MgB_2, and NCA + AlB_2. All the samples contain the $LiPF_6$(EC/DEC/EMC) electrolyte,

Since T_{on} of NCA|$LiPF_6$(EC/DEC)|AG was relatively low and the NCA electrode was the main cause for the thermal runaway, we tried to improve the thermal stability of NCA. Fig. 5 shows the DSC curves for NCA, NCA + MgB_2, and NCA + AlB_2, because electrical conductivities of MgB_2 and AlB_2 are relatively high [28,29]. Note that electrolyte additives such as LiBOB are effective for improving the thermal stability of AG [22,23], but not effective for positive electrodes such as NCA and NCM [12,13]. The Li composition (x) in $Li_xNi_{0.8}Co_{0.15}Al_{0.05}O_2$ for the DSC analyses was 0.34(1). In addition, we confirmed that the C/D curves when including MgB_2 or AlB_2 powder are essentially the same as those for the conventional NCA (not shown), up to current density of 2 $mA \cdot cm^{-2}$. The thermal stability of NCA is clearly improved by adding MgB_2 or AlB_2 powder. That is, the T of the maximum heat flow is 264 (257) °C for MgB_2 (AlB_2), which is ~14 (7) °C higher than that of the conventional NCA. Furthermore, the value of the maximum heat flow is decreased to 2.66 $W \cdot g^{-1}$ for MgB_2 and 2.84 $W \cdot g^{-1}$ for AlB_2, with respect to 4.32 $W \cdot g^{-1}$ for the conventional NCA. Although origins for such improvements are currently unknown, the formation of a solid-electrolyte interphase on NCA particles would prevent the oxidation of the EC/DEC/EMC solvent, because compounds containing boron are used in all-solid-state LIBs for a nanoscale interfacial modification [30]. Oxidation reactions of the MgB_2 (AlB_2) powder can be considered as another possibility. Further ARC and DSC studies combined with surface analyses could unveil details of the thermal stability of the NCA + MgB_2 and NCA + AlB_2 electrodes.

4. Conclusions

By using the AIM method, we performed ARC studies on NCA|$LiPF_6$(EC/DEC)|AG and NCM|$LiPF_6$(EC/DEC)|AG cells. The oxidation reaction of the EC/DEC solvent triggers the thermal runaway for the former cell, whereas the formation of LiF is the trigger for the latter cell. Thus, to suppress thermal runaway in LIBs, we first should consider whether the positive or the negative electrode material governs the thermal runaway. The AIM method is found to be effective for this purpose. We also succeeded in improving the thermal stability of NCA by using electrode additives such as MgB_2 and AlB_2. This approach is basically different from using conventional electrolyte additives such as LiBOB, in terms of efficacy for positive electrodes. Further ARC and DSC studies on various LIBs are underway in our laboratory.

References

[1] T.M. Bandhauser, S. Garimella, T.F. Fuller, A critical review of thermal issues in lithium-ion batteries, J. Electrochem. Soc. 158 (2011) R1–R25.
[2] P. Ping, Q. Wang, P. Huang, J. Sun, C. Chen, Thermal behaviour analysis of lithium-ion battery at elevated temperature using deconvolution method, Appl. Energy 129 (2014) 261–273.
[3] C.F. Lopez, J.A. Jeevarajan, P.P. Mukherjee, Experimental analysis of thermal runaway and propagation in lithium-ion battery modules, J. Electrochem. Soc. 162 (2015) A1905–A1915.
[4] C.F. Lopez, J.A. Jeevarajan, P.P. Mukherjee, Characterization of lithium-ion battery thermal abuse behavior using experimental and computational analysis, J. Electrochem. Soc. 162 (2015) A2163–A2173.
[5] S.V. Sazhin, E.J. Dufek, K.L. Gering, Enhancing Li-ion battery safety by early detection of nascent internal shorts, J. Electrochem. Soc. 164 (2017) A6281–A6287.
[6] S. Wilke, B. Schweitzer, S. Khateeb, S. Al-Hallaj, Preventing thermal runaway propagation in lithium ion battery packs using a phase change composite material: an experimental study, J. Power Sources 340 (2017) 51–59.
[7] D.I. Townsend, J.C. Tou, Thermal hazard evaluation by an accelerating rate calorimeter, Thermochim. Acta 37 (1980) 1–30.
[8] D.D. MacNeil, L. Christensen, J. Landucci, J.M. Paulsen, J.R. Dahn, An autocatalytic mechanism for the reaction of Li_xCoO_2 in electrolyte at elevated temperatures, J. Electrochem. Soc. 147 (2000) 970–979.
[9] D.D. MacNeil, J.R. Dahn, Test of reaction kinetics using both differential scanning and accelerating rate calorimetries as applied to the reaction of Li_xCoO_2 in non-aqueous electrolyte, J. Phys. Chem. A 105 (2001) 4430–4439.
[10] L. Ma, M. Nie, J.R. Dahn, A systematic study on the reactivity of different grades of charged $Li[Ni_xMn_yCo_z]O_2$ with electrolyte at elevated temperatures using accelerating rate calorimetry, J. Power Sources 327 (2016) 145–150.
[11] D.D. MacNeil, T.D. Hatchard, J.R. Dahn, A comparison between the high temperature electrode/electrolyte reactions of Li_xCoO_2 and $Li_xMn_2O_4$, J. Electrochem. Soc. 148 (2001) A663–A667.
[12] J. Jiang, J.R. Dahn, ARC studies of the thermal stability of three different cathode materials: $LiCoO_2$; $Li[Ni_{0.1}Co_{0.8}Mn_{0.1}]O_2$; and $LiFePO_4$, in $LiPF_6$ and LiBoB EC/DEC electrolytes, Electrochem. Commun. 6 (2004) 39–43.
[13] G.-Y. Kim, J.R. Dahn, ARC studies of the effects of electrolyte additives on the reactivity of delithiated $Li_{1-x}[Ni_{1/3}Mn_{1/3}Co_{1/3}]O_2$ and $Li_{1-x}[Ni_{0.8}Co_{0.15}Al_{0.05}]O_2$ positive electrode materials with electrolyte, J. Electrochem. Soc. 161 (2014) A1394–A1398.
[14] Y. Wang, J. Jiang, J.R. Dahn, The reactivity of delithiated $Li(Ni_{1/3}Co_{1/3}Mn_{1/3})O_2$, $Li(Ni_{0.8}Co_{0.15}Al_{0.05})O_2$ or $LiCoO_2$ with non-aqueous electrolyte, Electrochem. Commun. 9 (2007) 2534–2540.
[15] G.-Y. Kim, J.R. Dahn, Effects of electrode density on the safety of NCA positive electrode for Li-ion batteries, J. Electrochem. Soc. 160 (2013) A1108–A1111.
[16] S. El Khakani, D. Rochefort, D.D. MacNeil, ARC study of $LiFePO_4$ with different morphologies prepared via three synthetic routes, J. Electrochem. Soc. 163 (2016) A1311–A1316.
[17] H. Maleki, J.N. Howard, Role of the cathode and anode in heat generation of Li-ion cells as a function of state of charge, J. Power Sources 137 (2004) 117–127.
[18] P. Röder, N. Baba, H.-D. Wiemhöfer, A detailed thermal study of a $Li[Ni_{0.33}Co_{0.33}Mn_{0.33}]O_2$/$LiMn_2O_4$-based lithium ion cell by accelerating rate and differential scanning calorimetry, J. Power Sources 248 (2014) 978–987.
[19] M.N. Richard, J.R. Dahn, Accelerating rate calorimetry study on the thermal stability of lithium intercalated graphite in electrolyte I. Experimental, J. Electrochem. Soc. 146 (1999) 2068–2077.
[20] J. Jiang, J. Chen, J.R. Dahn, Comparison of the reactions between $Li_{7/3}Ti_{5/3}O_4$ or LiC_6 and nonaqueous solvents or electrolytes using accelerating rate calorimetry, J. Electrochem. Soc. 151 (2004) A2082–A2087.
[21] J. Jiang, J.R. Dahn, Dependence of the heat of reaction of $Li_{0.81}C_6$ (0.1 V), $Li_7Ti_5O_{12}$ (1.55 V), and $Li_{0.5}VO_2$ (2.45 V) reacting with nonaqueous solvents or electrolytes on the average potential of the electrode material, J. Electrochem. Soc. 153 (2006) A310–A315.
[22] T. Inoue, K. Mukai, Are all-solid-state lithium-ion batteries really safe?—verification by differential scanning calorimetry with an all-inclusive microcell, ACS Appl. Mater. Interfaces 9 (2017) 1507–1515.
[23] T. Ohzuku, A. Ueda, Phenomenlogical expression of solid-state redox potentials of $LiCoO_2$, $LiCo_{1/2}Ni_{1/2}O_2$, and $LiNiO_2$ insertion electrodes, J. Electrochem. Soc. 154 (2007) A314–A321.
[24] N. Yabuuchi, Y. Makimura, T. Ohzuku, Solid-state chemistry and electrochemistry of $LiCo_{1/3}Ni_{1/3}Mn_{1/3}O_2$ for advanced lithium-ion batteries III. Rechargeable capacity and cycleability, J. Electrochem. Soc. 154 (2007) A314–A321.
[25] I. Belharouak, D. Vissers, K. Amine, Thermal stability of the $Li(Ni_{0.8}Co_{0.15}Al_{0.05})O_2$ cathode in the presence of cell components, J. Electrochem. Soc. 153 (2006) A2030–A2035.
[26] J. Yamaki, H. Takatsuji, T. Kawamura, M. Egashira, Thermal stability of graphite anode with electrolyte in lithium-ion cells, Solid State Ionics 148 (2002) 241–245.
[27] N. Yabuuchi, T. Ohzuku, Novel lithium insertion material of $LiCo_{1/3}Ni_{1/3}Mn_{1/3}O_2$ for advanced lithium-ion batteries, J. Power Sources 119–121 (2003) 171–174.
[28] J. Nagamatsu, N. Nakagawa, T. Muranaka, Y. Zenitani, J. Akimitsu, Superconductivity at 39 K in magnesium diboride, Nature 410 (2001) 63–64.
[29] X.J. Wang, T. Mori, I. Kuzmych-Ianchuk, Y. Michiue, K. Yubuta, T. Shishido, Y. Grin, S. Okada, D.G. Cahill, Thermal conductivity of layered borides: the effect of building defects on the thermal conductivity of $TmAlB_4$ and anisotropic thermal conductivity of AlB_2, APL Mater. 2 (2014) 046113.
[30] S. Ohta, J. Seki, Y. Yagi, Y. Kihira, T. Tani, T. Asaoka, Co-sinterable lithium garnet-type oxide electrolyte with cathode for all-solid-state lithium ion battery, J. Power Sources 265 (2014) 40–44.